Effect of the natural state of an elastic cellular membrane on tank-treading and tumbling motions of a single red blood cell

Ken-ichi Tsubota[1,*] and Shigeo Wada[2]
[1]*Department of Mechanical Engineering, Chiba University, 1-33 Yayoi, Inage, Chiba 263-8522, Japan*
[2]*Department of Mechanical Science and Bioengineering, Osaka University, 1-3 Machikane-yama, Toyonaka 560-8531, Japan*
(Received 5 August 2009; revised manuscript received 12 October 2009; published 20 January 2010)

A two-dimensional computer simulation model was proposed for tank-treading and tumbling motions of an elastic biconcave red blood cell (RBC) under steady shear flow. The RBC model consisted of an outer cellular membrane and an inner fluid; the membrane's elastic properties were modeled by springs for stretch/compression and bending to consider the membrane's natural state in a practical manner. Membrane deformation was coupled with incompressible viscous flow of the inner and outer fluids of the RBC using a particle method. The proposed simulation model was capable of reproducing tank-treading and tumbling motions of an RBC along with rotational oscillation, which is the transition between the two motions. In simulations using the same initial RBC shape with different natural states of the RBC membrane, only tank-treading motion was exhibited in the case of a uniform natural state of the membrane, and a nonuniform natural state was necessary to generate the rotational oscillation and tumbling motion. Simulation results corresponded to published data from experimental and computational studies. In the range of simulation parameters considered, the relative membrane elastic force versus fluid viscous force was ~1 at the transition when the natural state nonuniformity was taken into account in estimating the membrane elastic force. A combination of natural state nonuniformity and elastic spring constant determined that change in the RBC deformation at the transition is that from a large compressive deformation to no deformation, such as rigid body.

DOI: 10.1103/PhysRevE.81.011910 PACS number(s): 87.85.gf, 87.85.gp

I. INTRODUCTION

The motion of a red blood cell (RBC) under blood flow plays an important role in the rheological properties of blood and has received particular attention for many years. With experimental measurements of mechanical behaviors of RBCs [1,2], computational modeling and simulations are indispensable for quantitative identification of RBC mechanics under blood flow and in establishing the multiscale mechanics of blood flow from microscopic blood cells to macroscopic rheologies in a blood vessel network [1,3–5].

Recent advances in computer simulation models enable us to consider the details of elastic deformation of a liquid capsule enclosed by an elastic membrane, including an RBC, during capsule motion [6–20], while analytical models have been created for a prescribed capsule shape in a certain flow field [21]. Continuum models, in most of which a single RBC is divided into an outer elastic membrane and an inner viscous fluid, successfully express RBC motion under shear flow observed in *in vitro* experiments [22–24]. The motion is characterized by the so-called tank-treading motion, defined as steady membrane rotation with constant shape and inclination angle, and tumbling motion, defined as overall rotation of an RBC. The transition between these two types of motion is observed as a rotational oscillation of the entire RBC accompanied by tank-treading motion [25,26].

It has been indicated that the motion of RBCs depends on the shear rate, the viscosity ratio between the inner and outer fluids of RBCs, the material properties of the elastic membrane and other physical constants [6,8,9,11–13,16–19,21]. This dependence is based on the fact that physical parameters determine the mechanical state of RBCs. In this sense, a natural state of the RBC membrane, which is defined as a reference configuration of the membrane at the zero-stress state, plays a key role in the mechanical state of RBCs. This is closely related to reports that motion of the liquid capsule enclosed by the elastic membrane is greatly affected by the resting capsule shape, which is defined as the capsule shape in the zero-stress state [6,11,12,16–18,27]. The effects of the resting shape, however, include mixed effects of the natural state of the membrane and the capsule shape, such as those represented by the surface-to-volume ratio, and thus, the role of the membrane's natural state in the motion of an RBC has not been identified yet.

The membrane structure of a normal biconcave RBC can be statically indeterminate because of membrane elastic forces and transmural pressure [27]. According to experimental observation of a shape memory phenomenon in a human RBC [28], the elastic energy of the RBC membrane reaches a minimum at a certain membrane position. This experimental evidence suggests that the natural state of the RBC membrane is similar to the configuration of a biconcave discoid shape. To gain quantitative understanding of the relationships between the membrane's natural state and RBC motion, it is useful to construct a computational model for examining the various conditions of the natural state of the membrane, as has been done to investigate the effects of prestress of the elastic membrane on capsule deformation in a flow field [9,14,15].

In this study, we propose a two-dimensional computer simulation model of an RBC's motion to examine the effects of the natural state of an elastic RBC membrane on tank-treading and tumbling motions under steady shear flow. A

*FAX: +81(43)290-3229; tsubota@faculty.chiba-u.jp

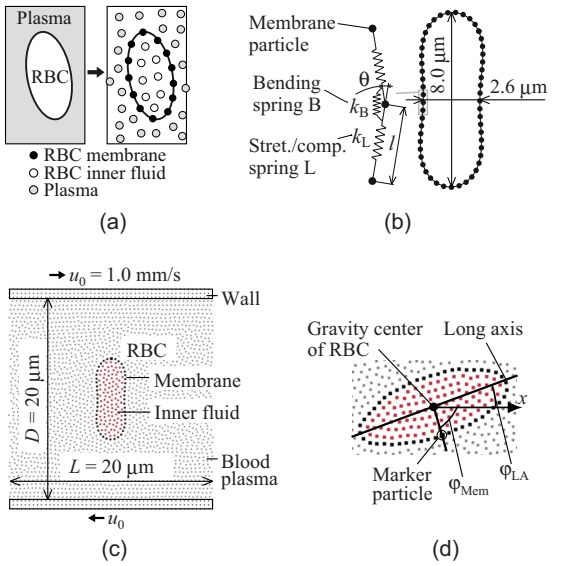

FIG. 1. (Color online) Computer simulation model of RBC motion under simple shear flow with particle method. (a) RBC and plasma as blood components, each of which is expressed by an assembly of computed particles. (b) Spring model of elastic RBC membrane. Stretch/compression and bending springs connect particles assigned to the RBC membrane. (c) Simulation model of a single RBC under shear flow. The model consists of RBC, blood plasma and rigid walls. (d) Definition of angle φ_{LA} for longitudinal direction of the entire RBC and φ_{Mem} for certain material points on the RBC membrane. Angles φ_{LA} and φ_{Mem} are used to quantify tank-treading and tumbling motions of the RBC in simulation results.

spring model is used for the elastic membrane to consider the distribution of the membrane's natural state in a practical manner, and a particle method is used to perform a coupled analysis of membrane elastic deformation and incompressible viscous flow of the RBC's inner and outer fluids. The RBC shape is initially set to biconcave with a transmural pressure, and different natural states of the membrane with the same initial shape are examined in numerical simulations of RBC motion.

II. METHODS

A. Two-dimensional particle model of blood

A two-dimensional problem with unit thickness h is assumed for blood flow, and an RBC and blood plasma are considered blood components, as shown in Fig. 1(a). The RBC is further divided into an outer cellular membrane and an inner fluid. An incompressible viscous flow is assumed for the blood plasma and RBC inner fluid, and an elastic deformation for the RBC membrane. All blood components are discretized by an assembly of computed particles depending on the type of component [10,29], in which each particle i has physical quantities such as position $\boldsymbol{r}_i$, velocity $\boldsymbol{u}_i$ and pressure p_i. Particles assigned to the RBC membrane, called membrane particles, have the averaged properties of the membrane and its neighboring fluid (blood plasma and RBC inner fluid) under a nonslip condition between them.

RBC membrane particles are connected with neighboring membrane particles by stretch/compression and bending springs to express the membrane's elastic properties in its natural state, as shown in Fig. 1(b) [29,30]. The elastic energy per unit thickness h stored in the stretch/compression springs due to the change in length l from its reference l_0 is expressed as

$$E_{\mathrm{L}} = \frac{k_{\mathrm{L}}}{2}\sum_{I=1}^{N}\left(\frac{l_I - l_0}{l_0}\right)^2, \tag{1}$$

where l_I denotes the length of stretch/compression spring element I, N is the total number of spring elements and k_{L} is the spring constant. The elastic energy stored in the bending springs is expressed as

$$E_{\mathrm{B}} = \frac{k_{\mathrm{B}}}{2}\sum_{I=1}^{N}\tan^2\left(\frac{\theta_I - \theta_I^0}{2}\right), \tag{2}$$

where θ_I denotes the angle of bending spring element I, θ_I^0 is the reference angle of the spring I, N is the total number of spring elements and k_{B} is the spring constant. In Eq. (2), θ_I is defined as the angle between two neighboring stretch/compression spring elements, and a tangential function is chosen to avoid folding of the bending springs. Spring constants k_{L} and k_{B} denote the spring energies per unit strain and angle, respectively. The reference length l_0 of the stretch/compression springs in Eq. (1) and the reference angle θ_I^0 of the bending springs in Eq. (2) are parameters representing a natural state of the elastic membrane. The spring force on each membrane particle i is calculated as

$$\boldsymbol{F}_i = -\frac{\partial W}{\partial \boldsymbol{r}_i}, \quad \text{where} \quad W = E_{\mathrm{L}} + E_{\mathrm{B}}, \tag{3}$$

on the basis of the principle of virtual work. In Eqs. (1) and (2), E_{L} and E_{B} represent elastic energies [N·m] per unit thickness $h=1$ m, and thus the units of E_{L}, E_{B}, k_{L}, and k_{B} are Newton [N].

B. Particle method for coupled analysis of fluid and membrane

To express an incompressible viscous flow, motions of all particles are determined by the moving particle semi-implicit (MPS) method, a particle method based on an equation of continuity and the Navier-Stokes (NS) equations [31]. For membrane particle i with unit thickness h, the elastic spring force in Eq. (3) is substituted into the particle's NS equation as the external force term,

$$\frac{D\boldsymbol{u}_i}{Dt} = -\frac{1}{\rho}\langle\nabla p\rangle_i + \frac{\mu}{\rho}\langle\nabla^2\boldsymbol{u}\rangle_i + \frac{h\boldsymbol{F}_i}{m_i}. \tag{4}$$

Equation (4) is the equation of motion to be solved for particle i, and fluid-membrane interaction is analyzed based on this equation. Here, $\langle\nabla p\rangle_i$ and $\langle\nabla^2\boldsymbol{u}\rangle_i$ denote the pressure gradient and velocity Laplacian models, respectively, used in the MPS method [31]. ρ and μ are the density and viscosity, respectively. In the third term on the right-hand side, the representative mass m_i of particle i is set to $h\rho d_0^2$, with d_0

being the mean distance between two neighboring computed particles.

C. Two-dimensional model of RBC motion in steady shear flow

Referring to *in vitro* experimental studies [23,24], a two-dimensional simulation model is created to investigate an RBC's motion under a steady shear flow, as shown in Fig. 1(c). The model consists of a single RBC, blood plasma and the upper and lower walls. The size of the model is $D=20$ μm in wall separation distance and $L=20$ μm in flow direction. A biconcave shape of the RBC, 8 μm in longitudinal length and 2.6 μm in the thickness of the concave part, is determined by numerical simulation of shape change of a swollen RBC due to decrease in its volume using a spring network model [29,30], the details of which are shown in Appendix A. The area of the biconcave RBC is 70% of that of a circle 6.0 μm in diameter, which is the shape of the swollen RBC model, and the membrane perimeter is the same as that of the circular swollen RBC, taking membrane incompressibility into account. The biconcave RBC is placed at the center of the simulation model, as shown in Fig. 1(c). As a boundary condition, the upper and lower wall are moved to the left and right, respectively, at a constant velocity $u_0=1.0\times10^{-2}$ m/s to generate a simple shear flow. A periodic boundary condition is applied to the left and right sides of the model. The viscosity μ_{Out} and density ρ of the blood plasma are 1.0×10^{-3} Pa·s and 1.0×10^{3} kg/m^3, respectively, which are the same as those of water and close to actual blood plasma properties. For the RBC inner fluid, the viscosity μ_{In} is set to five times the outer value μ_{Out} with the same density ρ, and therefore the viscosity ratio of the inner and outer RBC fluids, $\mu'=\mu_{\mathrm{In}}/\mu_{\mathrm{Out}}$, is fixed at 5, like that of actual RBCs. With these parameters, the shear rate, $\dot{\gamma}=2u_0/D$, is 1000, and the Reynolds number, $\mathrm{Re}=\rho u_0 D/\mu_{\mathrm{Out}}$, is 0.2.

In the two-dimensional simulation model, an original three-dimensional RBC deformation consisting of planar shear and out-of-plane bending is simplified to bending deformation. The ratio of the two spring constants, k_{L} and k_{B} in Eqs. (1) and (2), of the RBC membrane are set to be constant, $k_{\mathrm{L}}:k_{\mathrm{B}}=10:1$, to impose a constraint condition of a constant membrane perimeter that represents incompressibility of the RBC membrane [32]. As another constraint condition, the area of the inner fluid of the RBC is kept constant to consider a condition of constant RBC volume. In numerical simulations of RBC motion with the MPS method [31], the number of computed particles of the inner fluid of the RBC is always constant, ensuring a constant area of the inner fluid of the RBC.

By preliminary computer simulations, we confirmed that the relative effect of the fluid viscous force of the blood plasma on the elastic bending force of the RBC membrane is a key parameter in determining the RBC's motion at low-Reynolds number Re in the range $\sim10^{1}$ to $\sim10^{-2}$. This parameter is denoted as $\mu_{\mathrm{Out}}l_{\mathrm{RBC}}^2R_{\mathrm{RBC}}\dot{\gamma}/(k_{\mathrm{B}}l_0)$, of which the details are shown in Appendix B, with $l_{\mathrm{RBC}}=10$ μm and $R_{\mathrm{RBC}}=2.5$ μm being the characteristic length and radius of curvature of the RBC, respectively. The parameter is similar to a capillary number, which is defined as viscous force relative to surface tension. In this study, the parameter $\mu_{\mathrm{Out}}l_{\mathrm{RBC}}^2R_{\mathrm{RBC}}\dot{\gamma}/(k_{\mathrm{B}}l_0)$ is called the bending capillary number $\mathrm{Ca_B}$, and simulations of RBC motion are parametrically conducted for different $\mathrm{Ca_B}$ values ranging from 5 to 0.05 by changing k_{B} from 2.0×10^{-11} to 2.0×10^{-9} N. This range of $\mathrm{Ca_B}$ values is equivalent to that of shear rates $\dot{\gamma}$ from 366 to 3.66 with bending spring constant $k_{\mathrm{B}}=7.3\times10^{-12}$ N, corresponding to a bending modulus $B=1.8\times10^{-19}$ N·m [32]. Details of the relationship between bending spring constant k_{B} and bending modulus B are shown in Appendix A

The mean distance d_0 between computed particles is 0.4 μm, and the number of particles is about 2700. For the elastic membrane model of the RBC, the reference length l_0 in Eq. (1) of all stretch/compression springs is 0.4 μm, the same as the mean particle distance d_0. The reference angle θ_I^0 of the bending spring in Eq. (2) determines a natural state of the two-dimensional membrane and is therefore another key parameter determining the RBC's motion. Therefore, simulations of RBC motion are conducted for different magnitudes and distributions of θ_I^0. The number of springs N in Eqs. (1) and (2) is 48 for both stretch/compression and bending springs.

The same biconcave shape is maintained under no fluid force for all simulation parameters considered in the next section. In the biconcave shape, forces due to membrane stretch/compression and bending springs are balanced by those due to transmural pressure, and residual forces on the membrane of the RBC can be changed according to the simulation parameters, as briefly explained in Appendix A In the simulation results, RBC motions are characterized as tank-treading and tumbling motions. To quantify these motions, the x axis is set in the flow direction with its origin at the center of gravity of the RBC, and two angles are defined, as shown in Fig. 1(d). One is angle $\varphi_{\mathrm{Mem}}(-0.5\pi<\varphi_{\mathrm{Mem}}\leq0.5\pi)$ between the x axis and the line connecting the RBC's center of gravity and a certain material point on the membrane, as shown by a marker particle in Fig. 1(d). The other is angle $\varphi_{\mathrm{LA}}(-0.5\pi<\varphi_{\mathrm{LA}}\leq0.5\pi)$ between the x axis and the RBC's longitudinal axis. When periodic changes in φ_{Mem} and φ_{LA} are predicted, the periods T_{Mem} and T_{LA} are determined, respectively, by using the time average, and they are normalized by multiplying by the shear rate $\dot{\gamma}$. Time average of angle φ_{LA} is described as Φ_{LA}. For rotational oscillation, the time average of the rotation amplitude in angle is described as Φ_{OA}.

III. RESULTS

A. RBC motions for uniform natural state of elastic membrane

The reference bending angles θ_I^0 in Eq. (2) are set to zero for all bending springs I of the RBC membrane, and RBC motion simulations for different bending capillary numbers $\mathrm{Ca_B}$ from 5 to 0.05 are conducted. This assumes that a flat membrane shape corresponds to a natural state (zero-stress state) of the RBC membrane. The simulation results show tank-treading motion of the RBC membrane with constant

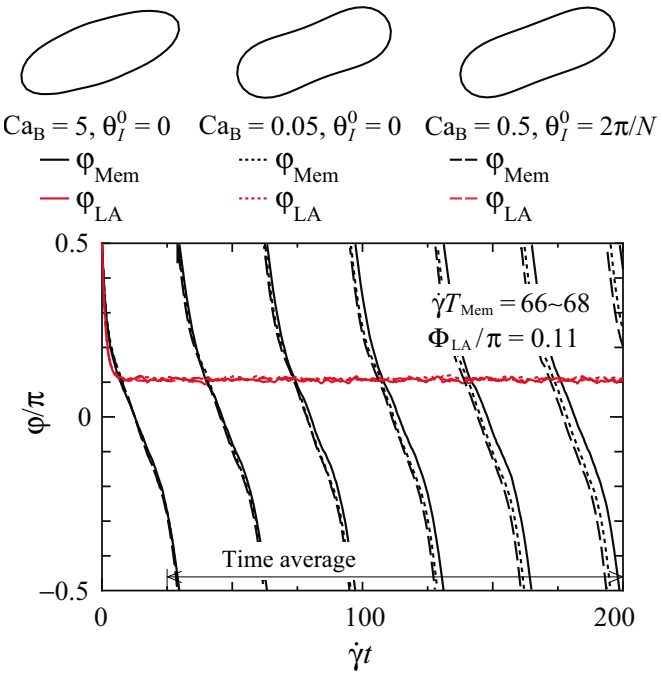

FIG. 2. (Color online) Simulation results of RBC motions in case of uniform natural state of the elastic RBC membrane. Line graphs show changes in angle φ_{LA}/π and φ_{Mem}/π for different sets of bending capillary number Ca_B and uniform reference angle θ_I^0, $(Ca_B, \theta_I^0)=(5,0)$, (0.05, 0) and $(0.5, 2\pi/N)$, as a function of normalized time $\dot{\gamma}t$. RBC shapes during tank-treading motions are illustrated for these parameter sets in the line graphs.

longitudinal angle $\Phi_{LA}=0.11\pi$ for all Ca_B values considered, as shown in Fig. 2, following clockwise rotation of the entire RBC in the initial simulation steps. The tank-treading motion is steady, as illustrated by periodic time-course changes in angle φ_{Mem}. The nondimensional period of tank-treading $\dot{\gamma}T_{Mem}$ is 66 to 68 and is not significantly affected by Ca_B. Ca_B dependence is observed only for RBC deformation, in that a greater Ca_B results in a more elongated RBC shape, as illustrated by the deformed shapes of RBCs at $(Ca_B, \theta_I^0)=(5,0)$ and (0.05, 0) in Fig. 2, according to the increase in fluid viscous force relative to membrane elastic force.

Reference bending angles θ_I^0 in Eq. (2) are set to a uniform $\theta_I^0=2\pi/N=0.04\pi$ for all bending springs I, and RBC motion simulations are conducted for $Ca_B=0.5$. This assumes that a circular RBC membrane, which is uniformly curved, corresponds to a natural state. The simulation result is the same as that with $\theta_I^0=0$ in terms of steady tank-treading motion with period $\dot{\gamma}T_{Mem}=66$ and constant longitudinal angle $\Phi_{LA}=0.11\pi$. Further simulations with different θ_I^0 values from 0.04π to 0.4π demonstrate that the results are not affected by θ_I^0 values as long as the same value is set for reference angle θ_I^0 of all bending springs I.

B. RBC motions for nonuniform natural state of elastic membrane

Reference bending angles θ_I^0 in Eq. (2) are distributed along the membrane as $-0.01\pi < \theta_I^0 \leq 0.11\pi$, as are those in the biconcave RBC shape at the initial state of the simulation [Fig. 1(b)], and RBC motion simulations for different bending capillary numbers Ca_B from 5 to 0.05 are conducted. This assumes that a biconcave membrane shape corresponds to a natural state (zero-stress state) of the RBC membrane. In this case, the RBC's motion depends on Ca_B, as shown in Fig. 3. When Ca_B is greater than 1, a rotational oscillation of the entire RBC occurs, accompanied by a tank-treading membrane motion, as illustrated by snapshots of RBC shapes for $Ca_B=1$ and line graphs of angles φ_{LA} and φ_{Mem} in Fig. 3(a). The amplitude Φ_{OA} and period T_{LA} of the RBC oscillation increase with decreasing Ca_B, as shown in Fig. 4. The oscillation period T_{LA} is half the tank-treading period T_{Mem}, reflecting π-rotational symmetry of the RBC shape [11,16,17,26]. Around $Ca_B=1$, the RBC's motion transits from rotational oscillation with membrane tank treading to a tumbling motion. In tumbling motion, an RBC is compressed around -0.3π to -0.5π in the longitudinal direction φ_{LA}, as illustrated by snapshots of RBC shapes from $\dot{\gamma}t=28$ to 31 in Fig. 3(b). The period T_{Mem} as a function of Ca_B takes the same values as T_{LA}, as shown in Fig. 4. This illustrates that tank-treading motion does not occur during tumbling motion. The degree of RBC deformation decreases with decreasing Ca_B, according to the decrease in the fluid viscous force relative to the membrane elastic force.

C. Effects of nonuniformity of natural state

The simulation results of Secs. III A and III B demonstrated that an RBC's motion depends on elastic behaviors according to nonuniform distribution of reference bending angle θ_I^0. Here, parameter α is introduced into Eq. (2) to represent the degree of natural state nonuniformity,

$$E_B = \frac{k_B}{2}\sum_{I=1}^{N} \tan^2\left(\frac{\theta_I - \alpha\theta_I^0}{2}\right) \quad (0 \leq \alpha), \tag{5}$$

and parametric simulations are conducted for different sets of bending capillary number Ca_B and natural state nonuniformity value α. In Eq. (5), $\alpha=0$ corresponds to a flat membrane in a natural state and $\alpha=1$ to the biconcave shape shown in Fig. 1(b). Moderate and excessive nonuniformity are denoted as $0<\alpha<1$ and $\alpha>1$, respectively.

According to bending capillary number Ca_B and natural state nonuniformity α, tank-treading and tumbling motions are exhibited, and a transition between the two occurs at a certain set of Ca_B and α values. For example, the transition occurs at $(Ca_B, \theta_I^0)=(5,3.5)$, (0.5, 0.5) and (0.05, 0.05). This illustrates that the natural state nonuniformity α at which the transition occurs increases with Ca_B. Compiling the results of parametric simulations for seven different Ca_B values, the parameter sets of Ca_B and α at which the transition occurs are plotted in Fig. 5 by open circles. This figure provides a phase diagram of an RBC's motion with respect to Ca_B and α and will be explained in terms of an elastic deformation of the RBC membrane in Sec. III D. RBCs at the transition are more compressed for a greater Ca_B value, as shown in Fig. 5, around -0.3π to -0.5π in the longitudinal direction φ_{LA} during tumbling motion. This demonstrates that a transition can occur with different degrees of RBC

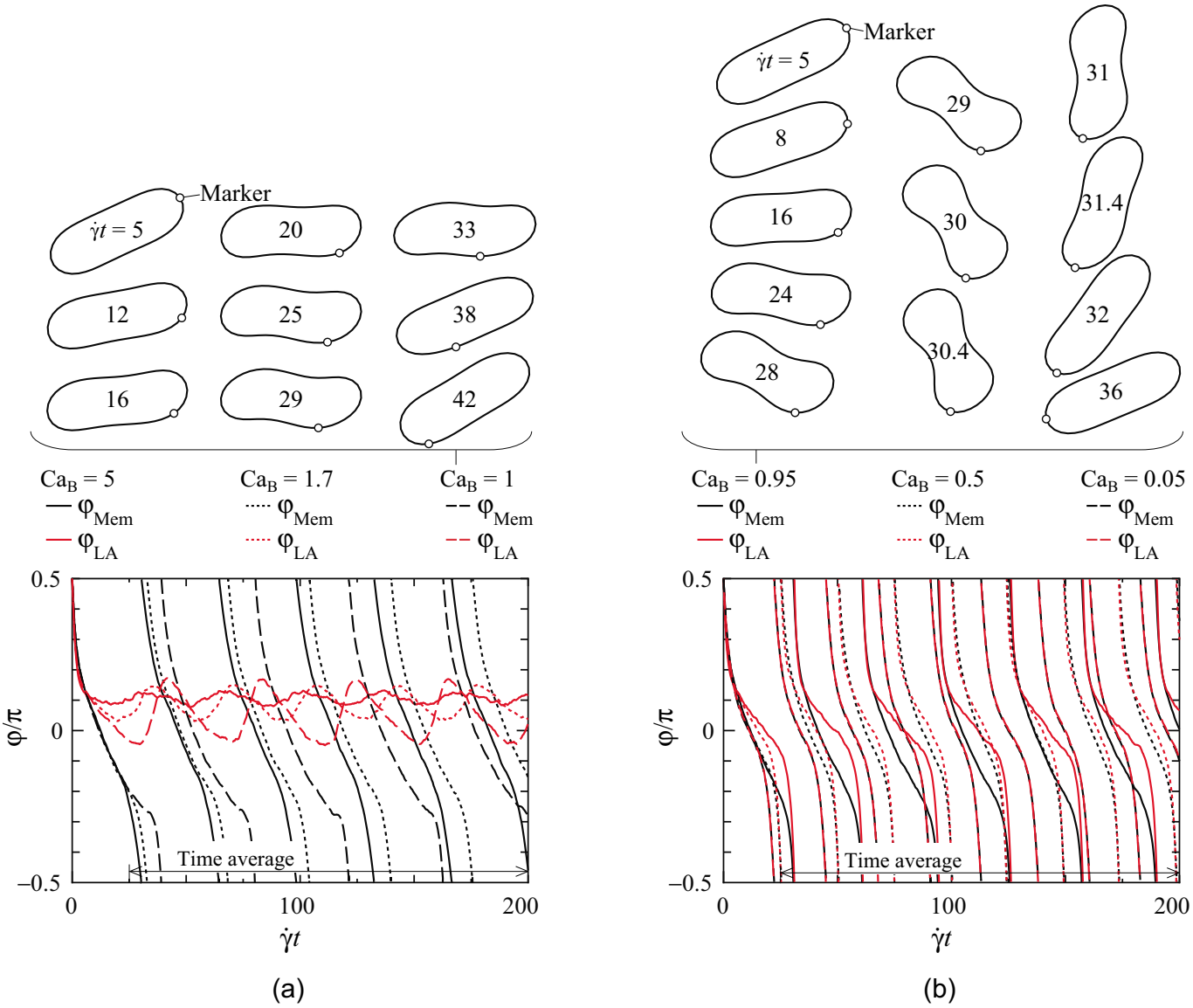

FIG. 3. (Color online) Simulation results of RBC motions in case of nonuniform natural state of the elastic RBC membrane. The membrane's natural state is assumed to be the biconcave shape shown in Fig. 1(b). (a) Rotational oscillation of the entire RBC with tank-treading motion exhibited for $Ca_B \geq 1$. Line graphs show changes in angle φ_{LA}/π and φ_{Mem}/π for $Ca_B=5$, 1.7 and 1 as a function of normalized time $\dot{\gamma}t$. The time-course of RBC shape changes is illustrated for $Ca_B=1$, in which the marker shows a certain material point on the membrane. (b) Tumbling motion of the entire RBC exhibited for $Ca_B<1$. Line graphs show changes in angle φ_{LA}/π and φ_{Mem}/π for $Ca_B=0.95$, 0.5 and 0.05 as a function of normalized time $\dot{\gamma}t$. The time course of RBC shape changes is illustrated for $Ca_B=0.95$, in which the marker shows a certain material point on the membrane.

deformation according to the combination of bending capillary number Ca_B and nonuniformity α of the membrane's natural state.

D. Elastic resistance force in RBC motion

The RBC motion simulations described in Sec. III C demonstrate that membrane residual forces at the same initial biconcave shape are affected by the natural state of the elastic membrane, leading to different RBC motions regulated by the elastic deformation of the membrane. In this section, the results of Sec. III C and Fig. 5 for the transition behavior between tank-treading and tumbling motions are explained in terms of the ratio of membrane elastic force to fluid viscous force [11]. Here, we assume steady tank-treading membrane motion along the given biconcave shape of Fig. 1(b); the elastic resistance force against the tank-treading motion per unit thickness is estimated from the additional elastic force generated because of the motion,

$$F_{Mem} = \frac{DW}{DL}, \tag{6}$$

where W is the elastic energy of the RBC membrane, as described in Eq. (3). The L $(0 \leq L < L_P)$ coordinate along the membrane for the total peripheral length L_P and the nondi-

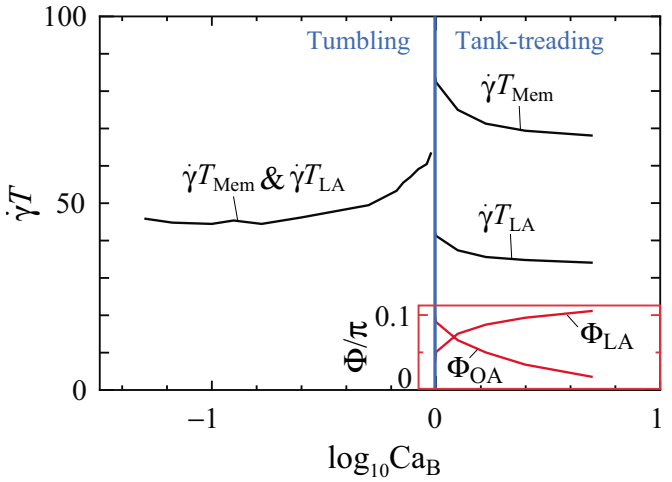

FIG. 4. (Color online) Average periods $\dot{\gamma}T$ and angles Φ/π that represent tank-treading and tumbling motions in case of a nonuniform natural state as a function of the logarithm of bending capillary number $\mathrm{Ca_B}$. Black lines show normalized periods $\dot{\gamma}T_{\mathrm{LA}}$ on angle φ_{LA} and $\dot{\gamma}T_{\mathrm{Mem}}$ on angle φ_{Mem} for a rotation (2π). Red (gray) inset in lower right shows angles for rotation amplitude Φ_{OA}/π and mean inclination angle Φ_{LA}/π of the entire RBC.

mensional coordinate $L^*=L/L_{\mathrm{P}}$ are defined as shown in Fig. 6. The sign of F_{Mem} denotes the resistance force against tank-treading motion ($F_{\mathrm{Mem}}>0$) and the driving force ($F_{\mathrm{Mem}}<0$). Since the stretch/compression springs have constant length, and the major deformation in this simulation is bending, only the bending energy E_{B} of elastic energy W contributes to elastic force F_{Mem} in Eq. (6). The total fluid viscous

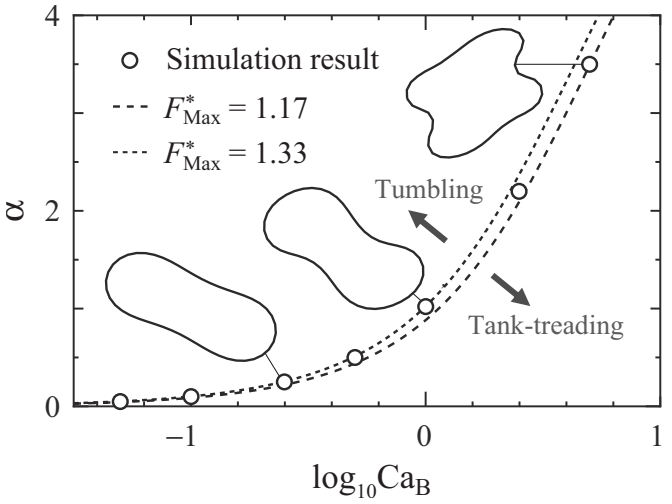

FIG. 5. Phase diagram of RBC tank-treading and tumbling motions with respect to the logarithm of bending capillary number $\mathrm{Ca_B}$ and natural state nonuniformity α. Open circles show the parameter sets at the transition between tank-treading and tumbling predicted by computer simulations. Dashed and dotted lines show transition lines from simple estimation of elastic force relative to the fluid force $F^*_{\mathrm{Max}}=1.17$ and 1.33, respectively. The force F^*_{Max} is estimated under the assumption of steady tank-treading motion; a detailed explanation of F^*_{Max} is found in Sec. III D. The $\mathrm{Ca_B}$ and α dependency of RBC deformation at the transition is also illustrated.

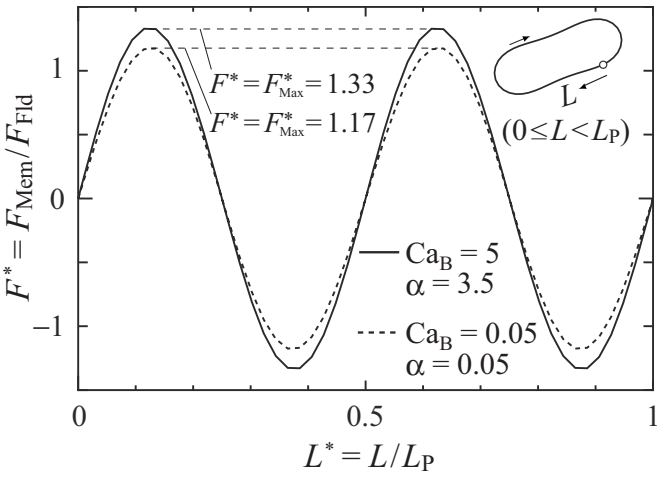

FIG. 6. Elastic resistance force, F_{Mem}, relative to fluid viscous force, F_{Fld}, estimated for a given membrane tank-treading motion for a prescribed biconcave shape under shear flow as a function of normalized peripheral length $L^*=L/L_{\mathrm{P}}$. Coordinate L is taken along the membrane periphery, and L_{P} is the total length of this periphery. The membrane configuration at the natural state completely matches the biconcave shape at $L^*=0$ (original position), 0.5 (half rotation) and 1 (full rotation). Solid and dotted lines show $F_{\mathrm{Mem}}/F_{\mathrm{Fld}}$ for $(\mathrm{Ca_B},\alpha)=(5,3.5)$ and (0.05, 0.05), respectively. F^*_{Max} is defined as the maximum value of $F_{\mathrm{Mem}}/F_{\mathrm{Fld}}$ during tank-treading motion, and is used in Fig. 5 to explain the simulation results of Sec. III C.

force on the RBC that drives tank-treading motion is roughly estimated as a constant value,

$$F_{\mathrm{Fld}}=\mu_{\mathrm{Out}}\dot{\gamma}l_{\mathrm{RBC}}. \tag{7}$$

The membrane elastic force relative to the fluid viscous force, $F^*=F_{\mathrm{Mem}}/F_{\mathrm{Fld}}$, during tank-treading motion is illustrated in Fig. 6 as a function of nondimensional coordinate L^* for the parameter sets $(\mathrm{Ca_B},\alpha)=(5,3.5)$ and (0.05, 0.05), at both of which the transition occurs in the simulations of Sec. III C. In the given tank-treading motion, an elastic resistance force is generated in accordance with elastic deformation of the membrane with nonuniform reference angles θ_i^0 of the bending springs. To maintain the tank-treading motion, the maximum value, F^*_{Max}, of relative elastic force F^* during the tank-treading pathway L^* should be less than a certain threshold value, which is roughly estimated to be on the order of unity. In the simulation results of Sec. III C, a transition between tank-treading and tumbling motions actually occurs at parameter sets $\mathrm{Ca_B}$ and α that correspond to F^*_{Max} values of from 1.17 to 1.33. Comparison of the curves corresponding to $F^*_{\mathrm{Max}}=1.17$ and 1.33 with simulation plots confirms that the transition simulated in Sec. III C can be explained by F^*_{Max} values, and that elastic behaviors influenced by the membrane's natural states play a key role in determining RBC motions. From the viewpoint of membrane elastic deformation, this graph also provides a good explanation for the recent numerical result that the motions of capsules with resting biconcave or elliptical shapes, which have a nonuniform natural state of the membrane, change from

tank-treading to tumbling motions when the bending stiffness of the membrane increases [16]. The F^*_{Max} value at the transition tends to decrease with bending capillary number $\mathrm{Ca_B}$, as shown in Fig. 5, and this result may suggest that large RBC deformation influencing outer fluid flow aids the transition from tank-treading to tumbling.

IV. DISCUSSION

A two-dimensional computer simulation model was proposed for tank-treading and tumbling motions of an RBC, taking the natural state of the elastic membrane into account. The results demonstrate that nonuniformity of the natural state of the elastic membrane plays an important role in an RBC's motion and deformation. Elastic properties have been regarded as an important factor in the deformation characteristics of RBCs, such as deformation into parachute and slipper shapes in a tube flow [22,33,34] and elliptical elongation in a steady shear flow [23,24]. The current study illustrates that elastic deformation plays an important role in overall RBC motions characterized as tank-treading and tumbling motions, in which the natural state of the elastic membrane is an essential consideration. Technically, the proposed simulation method provides a practical way to adjust the natural state of the elastic membrane, which is not easy in the shell model established using the finite element method [8,27].

Simulation results demonstrate that a transition can occur at different bending capillary numbers $\mathrm{Ca_B}$ with a certain natural state nonuniformity α, and that the degree of compressive deformation of the RBC increases with $\mathrm{Ca_B}$, as shown in Fig. 5. Therefore, the natural state and elastic constants of an RBC membrane have different roles in determining RBC deformation and motion. The results show good agreement with previously published experimental and computational studies in terms of compressive RBC deformation during tumbling motion [6,8,16], the tank-treading-to-tumbling transition according to the fluid viscous force relative to the membrane elastic force [11,13,16–18,26], increase in amplitude Φ_{OA} and period T_{LA} with decreasing $\mathrm{Ca_B}$ during overall RBC oscillation [11,13,16–18,26], and oscillation periods T_{OA} corresponding to half the values of the tank-treading period T_{Mem} [11,16]. Intermittent behavior of RBC motions, in which the two modes occur alternately, is predicted by a reduced model [11]. However, these motions are not obtained in the present study, which is consistent with the results obtained by a direct numerical simulation of an elastic capsule [18]. This evidence indicates that the tank-treading and tumbling motions are so sensitive to the membrane elastic behavior that under the strong influence of this behavior, the intermittency can be exhibited only in very narrow ranges of parameter space.

Simulation results of RBC motions in Sec. III are not significantly affected by viscous properties, as shown in Appendix C. The results shown in Fig. 4 do not change in the range of Reynolds number $\mathrm{Re}=\rho u_0 D/\mu_{\mathrm{Out}}$ of $\sim 10^{-2}$ to $\sim 10^{1}$. The viscosity ratio, $\mu'=\mu_{\mathrm{In}}/\mu_{\mathrm{Out}}$, of the inner and outer fluids of the RBC determines the characteristic periods of RBC motions, but does not affect their qualitative aspects. From a numerical view point, we note that the results shown in Sec. III have been converged with respect to the number of computed particles, as shown in Appendix D.

An RBC's deformation at the transition when natural state nonuniformity $\alpha=1$ is relatively small compared to three-dimensional simulation results [8]. This discrepancy is due to the two-dimensional modeling, in which planar shear deformation is not expressed, and the two-dimensional RBC in this study may be relatively stiff compared to a three-dimensional RBC. In the current two-dimensional model, RBC deformation is simplified to bending deformation, and it is impossible to put both membrane incompressibility and shear deformability on the two-dimensional membrane. Our two-dimensional model represents averaged properties of a three-dimensional RBC in the thickness direction, and thus, the simulation results indicate that the average of physical parameters in the thickness direction plays a key role in RBC motions regulated by elastic deformations. In this respect, the constraints of constant inner area and perimeter length in the present two-dimensional RBC model represent constraint characteristics averaged over the RBC volume, whereas a cross-section of the RBC, as well as its corresponding perimeter, in three dimensions can change during tank-treading and tumbling motions. On the other hand, fully three-dimensional modeling and simulation [35] are underway to quantify the membrane elastic constants and natural state separately by comparing simulation results to experimental observation [28]. Comparison of the present two-dimensional results and future three-dimensional ones will lead to understanding of the role of elastic deformation of an RBC in its tank-treading and tumbling motions. In addition, this point will lead to insight into a statically indeterminate membrane structure due to structural reorganization of molecules in the phospholipid bilayer and cytoskeleton [27,36–38]. Thus, it is also a necessary future work to measure the residual strain of cellular membranes directly, as has been done for other living tissues [39–42].

A blood flow field with multiple blood cells is affected by the motions of a single RBC simulated in this study. The proposed simulation model is applicable to blood flow with multiple RBCs [10] and provides a practical way to examine various conditions for hematocrit, flow velocity and vessel geometry with different diameters and branches [12,19,20,43–46]. According to the simulation results obtained in this study, the natural state of an RBC membrane would be an essential consideration in understanding multiscale mechanics of blood flow in a microvessel network system.

ACKNOWLEDGMENTS

This study was partially funded by a Grant-in-Aid for Scientific Research from the Ministry of Education, Culture, Sports, Science, and Technology, Japan.

APPENDIX A: SHAPE CHANGE SIMULATION OF RBC

Simulation of shape change in a swollen RBC due to a decrease in its volume is conducted on the basis of the spring network model [30]. The swollen RBC model has a circular

shape with diameter $\phi=6.0$ μm. In the shape change simulation, RBC membrane particles are moved so that the total elastic energy reaches a minimum by solving a set of motion equations for each particle,

$$m_S\ddot{\boldsymbol{r}}_i + \mu_S\dot{\boldsymbol{r}}_i = \boldsymbol{F}_i, \tag{A1}$$

by the finite difference method. Here, a dot $(\cdot)$ denotes the time derivative, and m_S and μ_S are the representative mass and viscosity of the RBC, respectively. Force $\boldsymbol{F}_i$ due to the total elastic spring energy is expressed as

$$\boldsymbol{F}_i = -\frac{\partial(W+\Gamma_A)}{\partial \boldsymbol{r}_i}, \tag{A2}$$

instead of Eq. (4), in order to introduce an areal constraint with penalty function Γ_A:

$$\Gamma_A = \frac{k_A}{2}\left(\frac{s-s_0}{s_0}\right)^2. \tag{A3}$$

Here, s and s_0 are the RBC's inner area and its reference value, respectively, and penalty constant k_A represents a spring constant of areal compressibility. The final RBC shape in the simulation depends on the magnitude of the volumetric decrease and the ratio among three spring constants, k_L, k_B, and k_A. Constants m_S and μ_S determine the process of shape changes but not the final shape. The biconcave RBC shown in Fig. 1(b) is the final shape obtained by the simulation in the case of 70% volumetric decrease from a swollen circular RBC with a spring constant ratio of $k_L:k_B:k_A=10:1:10^4$. In the condition of $k_L \gg k_B$, surface tension forces of the stretch/compression spring at the biconcave shape are much larger than bending spring forces. When the bending spring force is numerically decreased by changing spring constant k_B or natural state nonuniformity α in Eq. (5), changes in the surface tension force due to very small length changes in the stretch/compression springs compensate for the decreased bending force, and another equilibrium state of the elastic membrane is obtained with almost unchanged biconcave membrane shape. This is why the same initial biconcave shape is maintained even if the uniform reference angle θ_I^0 or natural state nonuniformity α are changed in Sec. III.

The bending spring constant k_B in Eq. (2) can be reduced to bending modulus B by comparing the bending elastic energy E_B in Eq. (2) with the analytically estimated E_B' from bending modulus B and membrane curvature C [30]. For a swollen circular RBC membrane with diameter $\phi=6.0$ μm, the bending energy E_B' per unit thickness is calculated by line integrals along the membrane peripherals $L=\phi\pi$ with the constant curvature $C=1/(\phi/2)$ as

$$E_B' = \frac{1}{2}B\int_L C^2 dL = \frac{1}{2}B\int_0^{\pi\phi}\left(\frac{1}{\phi/2}\right)^2 dL = \frac{2B\pi}{\phi}. \tag{A4}$$

The reported B value of 1.8×10^{-19} N·m [32] corresponds to $k_B=7.3\times10^{-12}$ N if reference angle θ_I^0 is taken as zero in Eq. (2).

APPENDIX B: BENDING CAPILLARY NUMBER Ca_B

In a membrane model with the bending spring of Eq. (2), $k_B\theta/4$, with bending spring constant k_B and bending angle θ, where angle θ is roughly approximated by $2l_0$ multiplied by the membrane curvature $1/R_{RBC}$, approximates the bending moments B/R_{RBC} of the elastic membrane. Here, l_0 is the reference length of stretch/compression springs in Eq. (1), and the order of bending modulus B can be denoted by k_Bl_0. In this study, the bending elastic force is represented by $k_Bl_0/(R_{RBC}l_{RBC})$, and bending capillary number $Ca_B=\mu_{Out}l_{RBC}^2R_{RBC}\dot{\gamma}/(k_Bl_0)$ is defined as the ratio of the representative fluid viscous force $\mu_{Out}\dot{\gamma}l_{RBC}$ to the bending elastic force $k_Bl_0/(R_{RBC}l_{RBC})$. Considering the RBC shape shown in Fig. 1(b), R_{RBC} is estimated to be around 1 to 4 μm. The characteristic lengths l_{RBC} and R_{RBC} of the RBC might be merged into only one length parameter with a suitable coefficient that represents the RBC's shape.

APPENDIX C: EFFECTS OF VISCOSITY ON RBC MOTIONS

With respect to the simulation results shown in Fig. 4, the effects of viscosity on RBC motions are investigated by numerical simulations, as shown in Fig. 7. Reynolds number, $Re=\rho u_0D/\mu_{Out}$, and viscosity ratio, $\mu'=\mu_{In}/\mu_{Out}$, between the inner and outer fluids of the RBC are considered as representative parameters of the viscosity.

Simulation results of characteristic periods, T_{Mem} and T_{LA}, and angles, Φ_{OA} and Φ_{LA}, of RBC motion as a function of bending capillary number Ca_B are illustrated in Fig. 7(a) for four cases of Re=0.02, 0.2, 2, and 20, of which Re=0.2 is used in Sec. III. Re is adjusted by changing the wall velocity u_0 in the simulations, and the viscosity ratio μ' is fixed at 5, as in Sec. III. It is possible that Re affects the inertial force of the entire RBC relative to the viscous one and the flow fields around the RBC. This might change the transition behaviors of RBC motion. In the simulations, however, no specific effect of Re on RBC motion appears in the range of Re considered in terms of two points. One point is that bending capillary number Ca_B is around 1 at the transition of RBC motions. The other is the pattern of increase and decrease in characteristic periods, T_{Mem} and T_{LA}, and angles, Φ_{OA} and Φ_{LA}, relative to bending capillary number Ca_B.

Figure 7(b) illustrates simulation results for four cases of viscosity ratio $\mu'=0.5$, 1, 2.5, and 5, of which $\mu'=5$ is used in Sec. III. The viscosity ratio μ' is adjusted by changing the inner viscosity μ_{In} in simulations, and the Reynolds number Re is fixed at 0.2, as in Sec. III. The simulation results demonstrate that a greater viscosity ratio μ' results in greater characteristic periods T_{Mem} and T_{LA}. In the range of μ' considered, the magnitudes of these periods are proportional to μ' values when $\mu'>1$, and the effects of μ' are gradual when $\mu'<1$. Characteristic angles, Φ_{OA} and Φ_{LA}, are not affected by μ'. Therefore, viscosity ratio μ' affects the characteristic period (or velocity, in other words) of RBC motions. The results for the four different μ' values are the same in terms of a Ca_B value around 1 at the RBC motion transition, and also in terms of the patterns of increase and

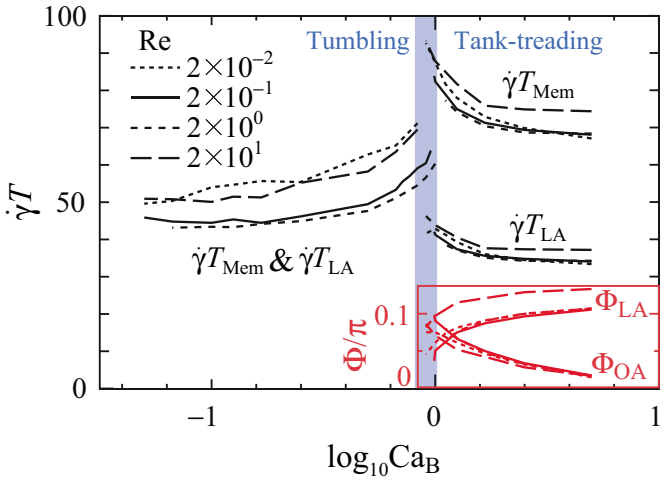

(a)

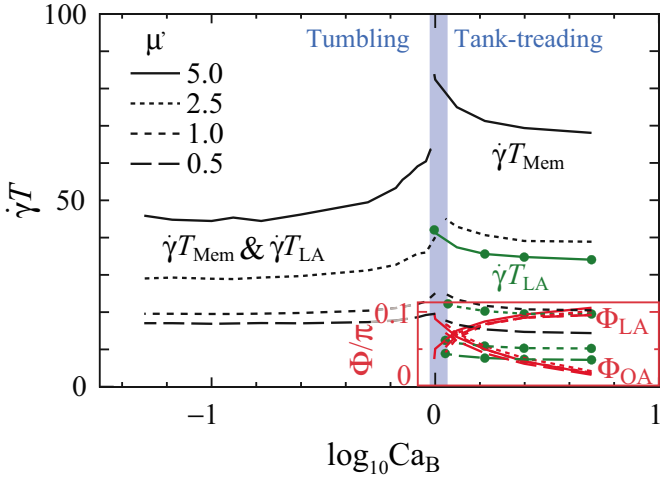

(b)

FIG. 7. (Color online) Effects of viscosity on simulation results of average periods $\dot{\gamma}T$ and angles Φ/π of RBC motions. (a) Reynolds number $\mathrm{Re}=\rho u_0 D/\mu_{\mathrm{Out}}$ of 0.02, 0.2, 2, and 20 and (b) viscosity ratio $\mu'=\mu_{\mathrm{In}}/\mu_{\mathrm{Out}}$ of 0.5, 1, 2.5, and 5 are examined as representative parameters of viscosity. Periods $\dot{\gamma}T$ and angles Φ/π are plotted as a function of the logarithm of bending capillary number $\mathrm{Ca_B}$, as in Fig. 4. Black lines show normalized periods $\dot{\gamma}T_{\mathrm{LA}}$ on angle φ_{LA} and $\dot{\gamma}T_{\mathrm{Mem}}$ on angle φ_{Mem} for a rotation (2π). Green (gray) lines with closed circles in (b) show $\dot{\gamma}T_{\mathrm{LA}}$. Red (gray) inset in lower right shows angles for rotation amplitude Φ_{OA}/π and mean inclination angle Φ_{LA}/π of the entire RBC. The simulation results of Re=0.2 in (a) and $\mu'=5$ in (b), indicated by solid lines, are the same as those used in Sec. III B, and thus, these solid lines illustrate the same results as those illustrated in Fig. 4.

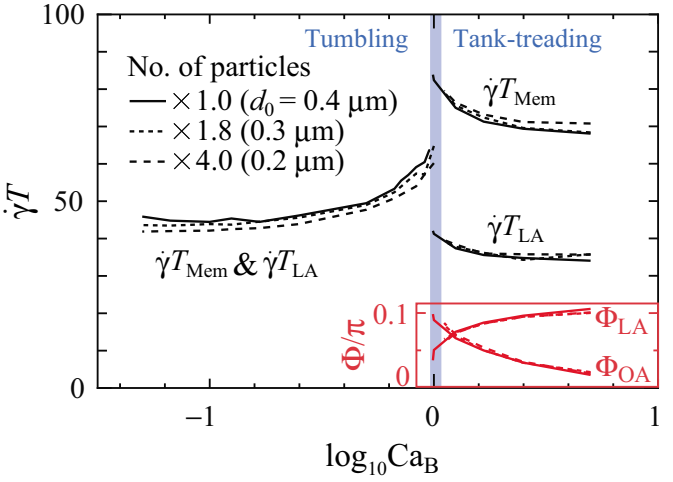

FIG. 8. (Color online) Effects of number of computed particles on simulation results of average periods $\dot{\gamma}T$ and angles Φ/π of RBC motions. Periods $\dot{\gamma}T$ and angles Φ/π, as a function of the logarithm of bending capillary number $\mathrm{Ca_B}$, are plotted for three cases: the same number of particles as that used in Sec. III B (×1.0), 1.8 times more particles (×1.8) and 4.0 times more particles (×4.0). The solid lines for (×1.0) illustrate the same result as that illustrated in Fig. 4. Black lines show normalized periods $\dot{\gamma}T_{\mathrm{LA}}$ on angle φ_{LA} and T_{Mem} on angle φ_{Mem} for a rotation (2π). Red (gray) inset in lower right shows angles for rotation amplitude Φ_{OA}/π and mean inclination angle Φ_{LA}/π of the entire RBC.

decrease in characteristic periods, T_{Mem} and T_{LA}, and angles, Φ_{OA} and Φ_{LA}, of RBC motion relative to bending capillary number $\mathrm{Ca_B}$.

APPENDIX D: EFFECTS OF NUMBER OF COMPUTED PARTICLES ON RBC MOTIONS

The characteristic periods, T_{Mem} and T_{LA}, and angles, Φ_{OA} and Φ_{LA}, of RBC motion as a function of bending capillary number $\mathrm{Ca_B}$ are illustrated in Fig. 8 for three cases of the number of computed particles: (1) the same number of computed particles as that used in Sec. III, (2) 1.8 times more computed particles and (3) 4.0 times more computed particles. Although some numerical artifacts exist, the results for the three cases are the same in terms of a $\mathrm{Ca_B}$ value around 1 at the RBC motion transition, and also in terms of the pattern of increase and decrease in characteristic periods, T_{Mem} and T_{LA}, and angles, Φ_{OA} and Φ_{LA}, of RBC motion relative to bending capillary number $\mathrm{Ca_B}$. The number of computed particles used in Sec. III is the smallest among the three cases, and thus it is confirmed that the results in Sec. III have converged with respect to the number of computed particles.

[1] A. R. Pries, T. W. Secomb, and P. Gaehtgens, Cardiovasc. Res. **32**, 654 (1996).
[2] K. J. Van Vliet, G. Bao, and S. Suresh, Acta Mater. **51**, 5881 (2003).
[3] M. Sugihara-Seki and B. M. Fu, Fluid Dyn. Res. **37**, 82 (2005).
[4] T. W. Secomb, D. A. Beard, J. C. Frisbee, N. P. Smith, and A. R. Pries, Microcirculation **15**, 693 (2008).
[5] J. Lee and N. P. Smith, Microcirculation **15**, 699 (2008).
[6] S. Ramanujan and C. Pozrikidis, J. Fluid Mech. **361**, 117 (1998).
[7] D. Barthès-Biesel, A. Diaz, and E. Dhenin, J. Fluid Mech. **460**, 211 (2002).
[8] C. Pozrikidis, Ann. Biomed. Eng. **31**, 1194 (2003).
[9] E. Lac and D. Barthès-Biesel, Phys. Fluids **17**, 072105 (2005).
[10] K. Tsubota, S. Wada, and T. Yamaguchi, J. Biomech. Sci. Eng. **1**, 159 (2006).
[11] J. M. Skotheim and T. W. Secomb, Phys. Rev. Lett. **98**, 078301 (2007).
[12] M. M. Dupin, I. Halliday, C. M. Care, L. Alboul, and L. L. Munn, Phys. Rev. E **75**, 066707 (2007).
[13] H. Noguchi and G. Gompper, Phys. Rev. Lett. **98**, 128103 (2007).
[14] Y. Lefebvre and D. Barthès-Biesel, J. Fluid Mech. **589**, 157 (2007).
[15] H. Luo and C. Pozrikidis, Int. J. Solids Struct. **44**, 8074 (2007).
[16] Y. Sui, Y. T. Chew, P. Roy, X. B. Chen, and H. T. Low, Phys. Rev. E **75**, 066301 (2007).
[17] Y. Sui, H. T. Low, Y. T. Chew, and P. Roy, Phys. Rev. E **77**, 016310 (2008).
[18] S. Kessler, R. Finken, and U. Seifert, J. Fluid Mech. **605**, 207 (2008).
[19] S. K. Doddi and P. Bagchi, Phys. Rev. E **79**, 046318 (2009).
[20] J. L. McWhirter, H. Noguchi, and G. Gompper, Proc. Natl. Acad. Sci. U.S.A. **106**, 6039 (2009).
[21] S. R. Keller and R. Skalak, J. Fluid Mech. **120**, 27 (1982).
[22] H. L. Goldsmith and J. Marlow, Proc. R. Soc. London, Ser. B **182**, 351 (1972).
[23] T. M. Fischer, M. Stöhr-Lissen, and H. Schmid-Schönbein, Science **202**, 894 (1978).
[24] T. M. Fischer, Biophys. J. **93**, 2553 (2007).
[25] V. Kantsler and V. Steinberg, Phys. Rev. Lett. **96**, 036001 (2006).
[26] M. Abkarian, M. Faivre, and A. Viallat, Phys. Rev. Lett. **98**, 188302 (2007).
[27] C. Pozrikidis, IMA J. Math. Appl. Med. Biol. **22**, 34 (2005).
[28] T. M. Fischer, Biophys. J. **86**, 3304 (2004).
[29] K. Tsubota, S. Wada, and T. Yamaguchi, Comput. Methods Programs Biomed. **83**, 139 (2006).
[30] S. Wada and R. Kobayashi, Trans. JSME, Ser. A **69**, 14 (2003).
[31] S. Koshizuka and Y. Oka, Nucl. Sci. Eng. **123**, 421 (1996).
[32] R. M. Hochmuth and R. E. Waugh, Annu. Rev. Physiol. **49**, 209 (1987).
[33] R. Skalak and P. I. Branemark, Science **164**, 717 (1969).
[34] P. Gaehtgens, C. Dührssen, and K. H. Albrecht, Blood Cells **6**, 799 (1980).
[35] K. Tsubota and S. Wada, Int. J. Mech. Sci. (to be published).
[36] N. S. Gov and S. A. Safran, Biophys. J. **88**, 1859 (2005).
[37] J. Li, G. Lykotrafitis, M. Dao, and S. Suresh, Proc. Natl. Acad. Sci. U.S.A. **104**, 4937 (2007).
[38] N. Mohandas and E. Evans, Annu. Rev. Biophys. Biomol. Struct. **23**, 787 (1994).
[39] Y. C. Fung, *Biodynamics: Circulation* (Springer, New York, 1984).
[40] Y. C. Fung and S. Q. Liu, Am. J. Physiol. **262**, H544 (1992).
[41] T. Adachi, M. Tanaka, and Y. Tomita, J. Biomech. Eng. **120**, 342 (1998).
[42] T. Matsumoto, T. Goto, T. Furukawa, and M. Sato, J. Biomech. **37**, 807 (2004).
[43] T. W. Secomb, B. Styp-Rekowska, and A. R. Pries, Ann. Biomed. Eng. **35**, 755 (2007).
[44] V. Vitkova, M. A. Mader, B. Polack, C. Misbah, and T. Podgorski, Biophys. J. **95**, L33 (2008).
[45] C. Sun and L. L. Munn, Biophys. J. **88**, 1635 (2005).
[46] L. L. Munn and M. M. Dupin, Ann. Biomed. Eng. **36**, 534 (2008).